Design of a Control Limiter to Improve the Dynamic Response of Energy Storage Systems

Álvaro Ortega, *Student Member, IEEE*, Federico Milano, *Senior Member, IEEE*

***Abstract*— This paper proposes an effective control scheme to improve the transient behavior of VSC-based energy storage systems facing energy saturations. This control is aimed to reduce abrupt transients following energy saturations of the storage device. The WSCC 9-bus test system is used for validating and discussing the proposed controller. In particular, the dynamic response of a battery energy storage undergoing energy saturations is tested considering deterministic as well as stochastic load variations. Simulation results shows that the proposed control scheme allows reducing installation costs while ensuring an adequate dynamic reponse of energy storage systems.**

***Index Terms*— Battery energy storage (BES), energy storage system (ESS), saturation, transient stability, voltage source converter (VSC).**

I. Introduction

In recent years, there has been a growing interest in the inclusion of Energy Storage Systems (ESSs) to the HV transmission systems. These devices can improve the stability of the system and increase the reliability of intermittent renewable power plants. The research in this field is currently exploring and testing several energy storage technologies [1]–[3]. The main issue with ESSs which greatly limits their installation is their high ratio cost vs. capacity. This fact has inspired several studies on optimal sizing and location of ESSs, mainly for long term dynamic analysis (see for example [4] and [5]). However, adjusting the size of the ESSs with the aim of reducing the installation costs may leads eventually to energy and/or power output saturations of the storage device that could cause abrupt transient phenomena in the system.

A large number of control strategies has been proposed for ESSs for medium and long term analysis (e.g., [6], [7]) and also for short time scale analysis (e.g., [8]–[10]). However, the number of researches on energy and power saturations of ESSs that are provided by the literature is limited (e.g., [11]–[13]). In [11], an anti-windup compensation method for ESSs to improve the saturation-dependent stability of power systems is designed using linear matrix inequality technique, whereas [12] presents a model predictive control approach designed to manage in real-time the power production of a grid-tied PV+ESS power plant with a reduced ESS capacity that can anticipate future saturations of the storage device. Finally, [13] discusses the modeling and data requirements of VSC-based Superconducting Magnetic Energy Storage (SMES) and Battery Energy Storage (BES) for power system stability simulations including realistic limitations of the storage devices, as well as those of the power electronic interfaces.

This paper proposes a simple and effective control strategy to improve the transient behavior of VSC-based ESSs facing energy saturations. The balanced, fundamental frequency model of the VSC that is proposed in [14] and [15] is used in this paper. This model includes dc circuit dynamics as well as an average quasi-static phasor model of the converter. The controller that is developed in this paper attempts to smooth the transients caused by the energy saturations of ESSs by gradually reducing the regulation capability of the storage control whenever the storage device is close to reach one of its energy limits, with the aim of getting to those limits following a smooth trajectory, and thus, avoiding saturation singularities. To minimize the degradation of the ESS performance resulting from energy saturation, the proposed control strategy is applied only if the ESS is close to its maximum storable energy and the storage device is charging, or if the energy is close to the minimum value and the ESS is discharging.

The paper is organized as follows. Section II describes the scheme of a generic VSC-based ESS. The controllers used in this paper as well as the model of a BES are also presented in this section. Section III depicts the structure and formulation of the proposed controller. The effectiveness of the controller is verified in Section IV through time domain simulations. All simulations are based on the WSCC 9-bus test system. Finally, Section V draws conclusions and outlines future work directions.

II. System Overview

Subsection II-A presents the elements that compose a generic ESS and the controllers that regulate its dynamic response. Since the case study considers a BES, the specific model of this device is presented in Subsection II-B.

A. ESS Topology and Detailed Control Scheme

Figure 1 shows the overall structure of an ESS connected to a grid through a VSC device. The objective of the ESS is to control a measured quantity w, e.g., the frequency of either a local bus or the Center of Inertia (COI), if available, or the power flowing through a transmission line. The elements shown in Fig. 1, except for the storage device, are common to all VSC-based ESSs.

Figure 2 illustrates the VSC scheme [16], [17]. The usual configuration includes a transformer, a by-directional converter and a condenser. The transformer provides galvanic insulation, whereas the condenser maintains the voltage level

This work was conducted in the Electricity Research Centre, University College Dublin, Ireland, which is supported by the Commission for Energy Regulation, Bord Gáis Energy, Bord na Móna Energy, Cylon Controls, EirGrid, Electric Ireland, Energia, EPRI, ESB International, ESB Networks, Gaelectric, Intel, and SSE Renewables. This publication has emanated from research conducted with the financial support of SFI.

Á. Ortega and F. Milano are with the School of Electrical, Electronic and Communications Engineering of the University College Dublin, Dublin, Ireland (e-mail: federico.milano@ucd.ie).

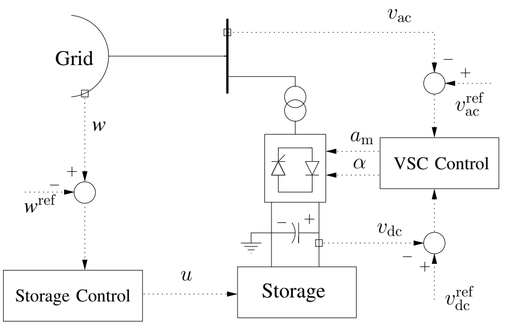

Fig. 1: Scheme of an ESS coupled to a grid.

at the dc side of the converter. The dc voltage is transformed to ac voltage by a proper control logic of the power electronics switches. The variables involved in this control logic are the modulation amplitude $a_{\rm m}$, and the firing angle α.

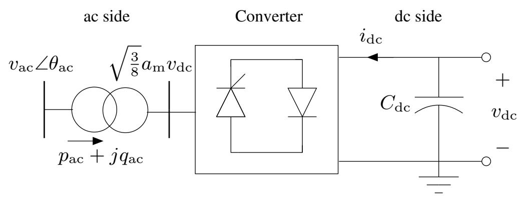

Fig. 2: Scheme of a Voltage Source Converter.

The equations of the ac side of the VSC depicted in Fig. 2 can be written as follows:

$$\begin{aligned} p_{\rm ac} &= \;\; g_{\rm t}v_{\rm ac}^2 - \kappa g_{\rm t}\cos(\theta_{\rm ac}-\alpha) - \kappa b_{\rm t}\sin(\theta_{\rm ac}-\alpha) \\ q_{\rm ac} &= -b_{\rm t}v_{\rm ac}^2 + \kappa b_{\rm t}\cos(\theta_{\rm ac}-\alpha) - \kappa g_{\rm t}\sin(\theta_{\rm ac}-\alpha) \end{aligned} \tag{1}$$

where $\kappa = \sqrt{\frac{3}{8}}a_{\rm m}v_{\rm dc}v_{\rm ac}$; and $g_{\rm t}+jb_{\rm t} = 1/(r_{\rm t}+jx_{\rm t})$ is the series admittance of the transformer. The power balance between the dc and the ac sides of the inverter is imposed by:

$$v_{\rm dc}i_{\rm dc} = g_{\rm t}\frac{3}{8}a_{\rm m}^2v_{\rm dc}^2 - \kappa g_{\rm t}\cos(\theta_{\rm ac}-\alpha) - \kappa b_{\rm t}\sin(\theta_{\rm ac}-\alpha) \tag{2}$$

Finally, the dc voltage dynamics is driven by the dc-link capacitor:

$$\dot{v}_{\rm dc} = -\frac{i_{\rm dc}}{C_{\rm dc}} \tag{3}$$

The modulation amplitude and the firing angle of the VSC are used for regulating the ac and dc voltages. These controllers are similar to those implemented in Statcom devices [14], [15]. For the sake of completeness, Figs. 3 and 4 depict the modulation amplitude and the firing angle control schemes, respectively.

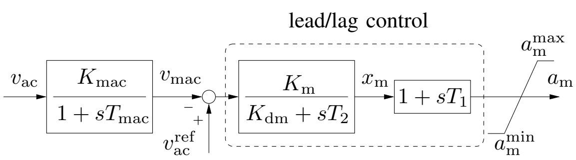

Fig. 3: Modulation amplitude controller of the VSC.

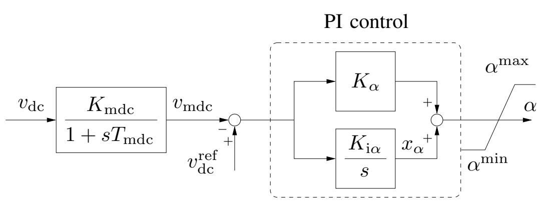

Fig. 4: Firing angle controller of the VSC.

The charge/discharge process of the storage device is regulated by the storage control (see Fig. 5). The input signal of the control is the error between the actual value of a measured quantity of the system, say w, and a reference value ($w - w^{\rm ref}$). If $w = w^{\rm ref}$, the storage device is inactive and its energy is constant. For $w \neq w^{\rm ref}$, the storage device injects active power into the ac bus through the VSC (discharge process) or absorbs power from the ac bus (charge process). A dead-band block is also included to reduce the sensitivity of the Storage Control to small changes of the measured signal w with respect to the given reference $w^{\rm ref}$ [18].

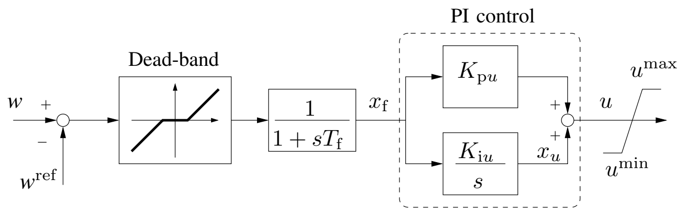

Fig. 5: Scheme of the storage control.

B. BES Model

A well-known model to represent the dynamics of a rechargeable battery cell is the Shepherd model [19]:

$$\begin{aligned} \dot{Q}_{\rm e} &= i_{\rm b}/3600 \\ \dot{i}_{\rm m} &= \frac{i_{\rm b}-i_{\rm m}}{T_{\rm m}} \\ 0 &= v_{\rm oc} - v_{\rm p}(Q_{\rm e}, i_{\rm m}) + v_{\rm e}e^{-\beta_{\rm e}Q_{\rm e}} - R_{\rm i}i_{\rm b} - v_{\rm b} \end{aligned} \tag{4}$$

where $Q_{\rm e}$ is the extracted capacity in Ah; $i_{\rm m}$ is the battery current $i_{\rm b}$ passed through a low-pass filter with time constant $T_{\rm m}$; $v_{\rm oc}$, $v_{\rm p}$ and $v_{\rm e}$ are the open-circuit, polarization and exponential voltages, respectively; $\beta_{\rm e}$ is the exponential zone time constant inverse; $R_{\rm i}$ is the internal battery resistance; and $v_{\rm b}$ is the battery voltage.

The variation of the polarization voltage $v_{\rm p}$ with respect to $i_{\rm m}$ and $Q_{\rm e}$ is given by:

$$v_{\rm p}(Q_{\rm e}, i_{\rm m}) = \begin{cases} \dfrac{R_{\rm p}i_{\rm m} + K_{\rm p}Q_{\rm e}}{\rm SOC} & \text{if} \quad i_{\rm m} > 0 \;\; \text{(discharge)} \\ \dfrac{R_{\rm p}i_{\rm m}}{q_{\rm e}+0.1} + \dfrac{K_{\rm p}Q_{\rm e}}{\rm SOC} & \text{if} \quad i_{\rm m} \leq 0 \;\; \text{(charge)} \end{cases} \tag{5}$$

where $R_{\rm p}$ and $K_{\rm p}$ are the polarization resistance and polarization constant, respectively; and SOC is the state of charge of the battery which is defined as:

$${\rm SOC} = \frac{Q_{\rm n}-Q_{\rm e}}{Q_{\rm n}} \tag{6}$$

Figure 6 depicts the connection of the BES to the VSC through a dc/dc converter (boost converter):

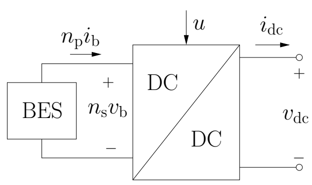

Fig. 6: Scheme of the BES and the boost converter.

The equations that describe the behavior of the dc/dc converter are as follows:

$$\begin{aligned} 0 &= (1-2u)v_{\rm dc} - n_{\rm s}v_{\rm b} \\ 0 &= i_{\rm dc} - (1-2u)n_{\rm p}i_{\rm b} \end{aligned} \tag{7}$$

where u is the duty cycle of the converter; and $n_{\rm p}$ and $n_{\rm s}$ are the number of parallel and series connected battery cells, respectively.

III. Proposed Storage Input Limiter

This paper proposes an additional control block for the scheme depicted in Fig. 5. In the following, this limiter is referred to as Storage Input Limiter (SIL), as depicted in Fig. 7.

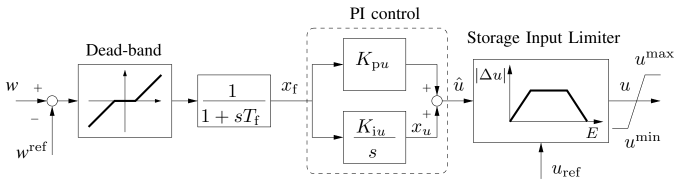

Fig. 7: Scheme of the storage control with the Storage Input Limiter block.

This block takes the actual value of the energy stored in the device, E, and regulates accordingly the input controlled variable of the storage device, u, as follows:

$$u = \begin{cases} \dfrac{E - E_{\min}}{E_{\min}^{\rm thr} - E_{\min}} \Delta u + u_{\rm ref} \\ \qquad \text{if} \quad E_{\min} \le E \le E_{\min}^{\rm thr} \quad \text{and} \quad \Delta u > 0 \\ \dfrac{E_{\max} - E}{E_{\max} - E_{\max}^{\rm thr}} \Delta u + u_{\rm ref} \\ \qquad \text{if} \quad E_{\max}^{\rm thr} \le E \le E_{\max} \quad \text{and} \quad \Delta u < 0 \\ \hat{u} \quad \text{otherwise} \end{cases} \tag{8}$$

where $u_{\rm ref}$ is the value of u such that the storage device is disabled; $\Delta u = \hat{u} - u_{\rm ref}$; $E_{\min}$ and $E_{\max}$ are the minimum and maximum storable energy in the ESS, respectively; and $E_{\min}^{\rm thr}$ and $E_{\max}^{\rm thr}$ define the minimum and maximum energy thresholds, respectively, that are computed as follows:

$$\begin{aligned} E_{\min}^{\rm thr} &= E_{\min} + \mu_{\min} \left(E_{\max} - E_{\min} \right) \\ E_{\max}^{\rm thr} &= E_{\max} - \mu_{\max} \left(E_{\max} - E_{\min} \right) \end{aligned} \tag{9}$$

where $\mu_{\min}$ and $\mu_{\max}$ are the coefficients that define the regions in which the SIL is operational. In this paper, we assume a symmetrical limiter, hence, $\mu_{\min} = \mu_{\max} = \mu$; where $\mu \in (0, 0.5]$.

The sign of Δu is taken into account in (8) with the aim of reducing its value, and hence altering the regulation capability of the Storage Control, only if the ESS is close to its maximum storable energy and the storage device is charging, or if the energy is close to the minimum value and the ESS is discharging. If any other condition is satisfied, the Storage Control is regulating as expected.

Particularizing the proposed SIL to the BES in Subsection II-B, it is straightforward to relate the energy and its limits in (8) and (9) to the SOC of the battery in (6). The output of the controller, u, is the duty cycle of the dc/dc converter in (7). Finally, if $\Delta u < 0$ the BES is charging, and if $\Delta u > 0$ discharging.

IV. Case Study

This section validates the proposed SIL through time domain simulations. With this aim, the WSCC 9-bus test system (see Fig. 8) is used for all simulations. This benchmark network consists of three synchronous machines, three transformers, six transmission lines and three loads. The system model also includes generator controllers such as primary voltage regulators (AVRs). The storage device considered in this paper is a 40MW BES and is connected to bus 8. All dynamic data of the WSCC 9-bus system as well as a detailed discussion of its transient behavior can be found in [20].

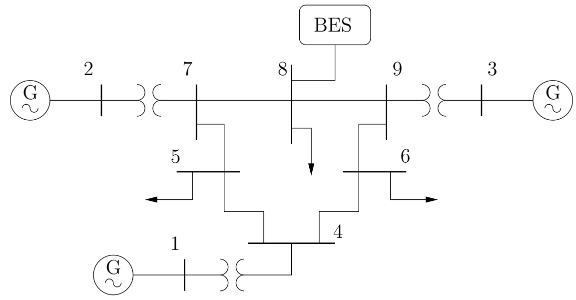

Fig. 8: WSCC 9-bus test system with an BES device connected to bus 8.

Two scenarios have been performed in this paper: Subsection IV-A shows the response of the WSCC system with a BES facing a deterministic variation of one load, whereas Subsection IV-B includes stochastic perturbations for all loads.

All simulations and plots have been obtained using DOME [21]. DOME has been compiled based on Python 2.7.5, CVXOPT 1.1.5, SuiteSparse 4.2.1, and Matplotlib 1.3.0; and has been executed by using a server mounting 48 CPUs, 256 GB of RAM and running a 64-bit Linux OS.

A. Deterministic Variation of Load

As an example of the performance of the proposed SIL when the BES reaches its maximum and minimum storable energy, Fig. 9 shows the response of the WSCC system in case of variations of the load. A loss of a 40MW load occurs at bus 5 at $t = 10$s, and is reconnected after 70s. Finally, a 50MW load is connected to bus 5 at $t = 130$s and is disconnected after 110s.

In this example, the frequency of the COI ($\omega_{\rm COI}$) of the system is regulated, and its performance is presented in Fig. 9(a). The $\omega_{\rm COI}$ signal can be obtained in real-time from the System Operator (e.g., EirGrid in Ireland). Note that the time-delays that may affect this signal are neglected in this paper since the varaitions of $\omega_{\rm COI}$ are relatively slow. In case the $\omega_{\rm COI}$ signal is not available, similar results are obtained by regulating the frequency at a local bus, e.g., the bus where the BESS is connected. It can be observed from Fig. 9(a) that without BES, the largest variation of the $\omega_{\rm COI}$ is around 1.8%. This variation is reduced by 50% when the BES is included in the system. Figure 9(a) also shows the effect of the energy saturations of the BES after about 40s (maximum level) and 150s (minimum level) of simulation. The inclusion of the SIL ($\mu = 0.2$) avoids the abrupt variations of the $\omega_{\rm COI}$ caused by these saturations.

The active power output of the BES with and without SIL is compared in Fig. 9(b). The SIL smooths the control of the input signal of the BES when is reaching one of its limits, and thus, avoids the steep decrease (increase) of the power consumed (injected) by the BES.

B. Stochastic Variation of Load

For this case study, stochastic perturbations have been considered for all loads. These stochastic processes have

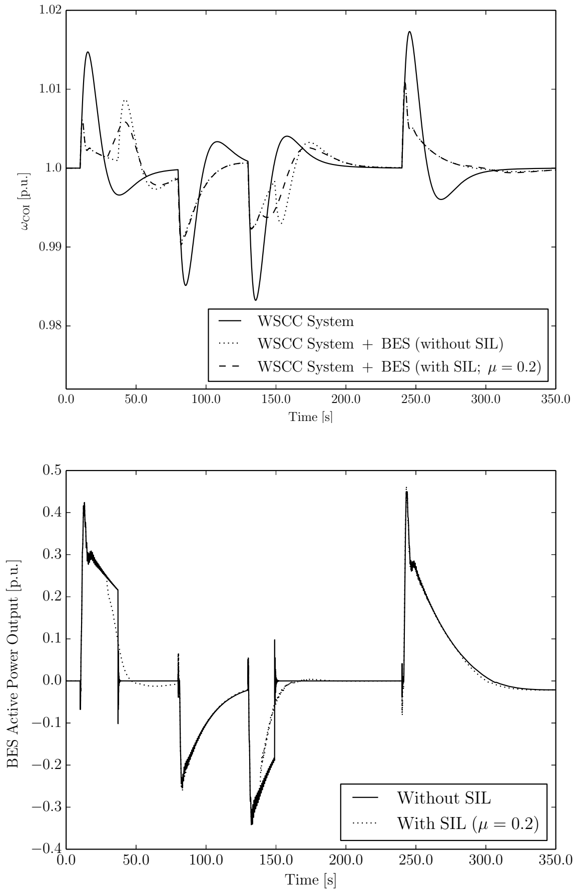

Fig. 9: Response of the WSCC system with a BES to deterministic variations of the load. (a) Frequency of the COI. (b) Active power output of the BES.

been modeled by using the Ornstein-Uhlenbeck's process, also known as *mean-reverting* process [22], [23]. For the sake of clarity, the stochastic load model used in this paper is defined by the following set of Stochastic Differential Algebraic Equations (SDAE):

$$\begin{aligned} p_{\rm L}(t) &= (p_{\rm L0} + \eta_p(t))(v(t)/v_0)^{\gamma} \\ \dot{\eta}_p(t) &= \alpha_p(\mu_p - \eta_p(t)) + b_p \xi_p \end{aligned} \tag{10}$$

where $p_{\rm L}$ is the active power of the loads, $p_{\rm L0}$ represents the initial active load power; v is the voltage magnitude at the bus where the load is connected; v_0 is the intial value of the bus voltage magnitude; exponent γ is a parameter that characterizes the dependence of the load with respect to voltage; η_p is the stochastic variable; α_p and b_p are the *drift* and *diffusion* of the stochastic process, respectively; μ_p is a pre-specified mean value; and ξ_p is the white noise. Similar equations are used to define the trajectories of load reactive powers. The interested reader can find a detailed description of this model in [23].

A step size of $h = 0.01$s has been used to generate the trajectories of the Wiener's process, and 2000 simulations are performed for each scenario. The initial load and generation levels are set by using an uniform distribution with $\pm 5\%$ of variation with respect to their original values. The step size for the time integration Δt is set to 0.1s, and the final simulation time is 200s.

As for the previous Subsection, the regulated variable is the frequency of the COI ($\omega_{\rm COI}$), and its evolution is represented

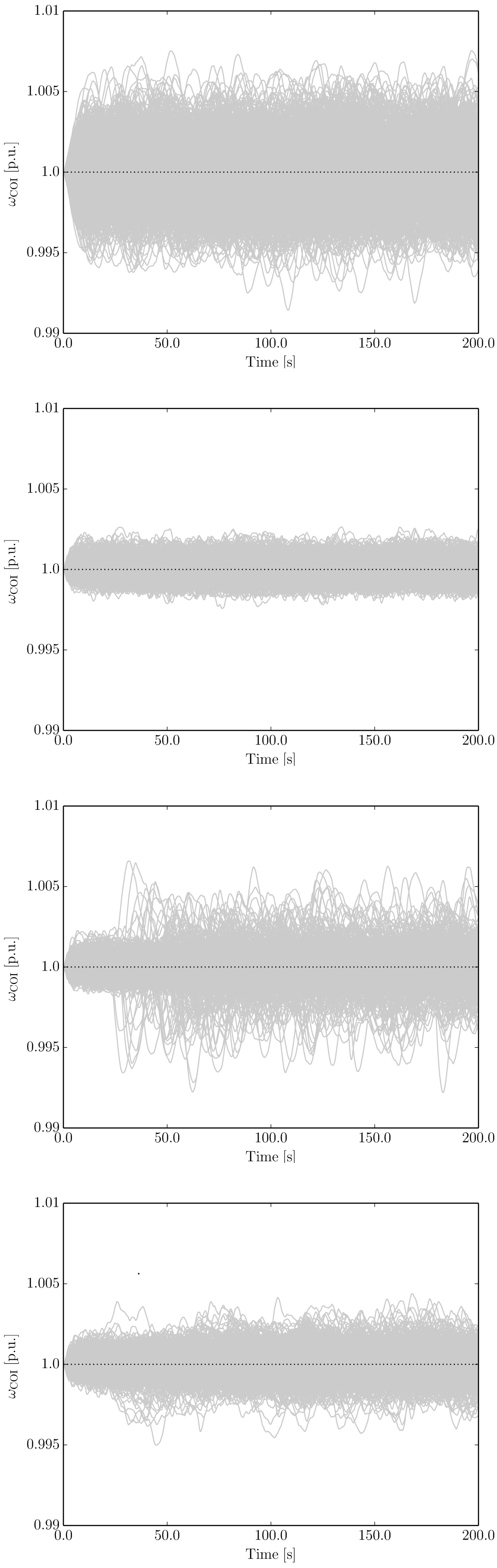

Fig. 10: Frequency of the COI when stochastic perturbations are considered for the loads. (a) WSCC System. (b) WSCC System + BES (oversized). (c) WSCC System + BES (without SIL). (d) WSCC System + BES (with SIL; $\mu = 0.2$)

in Fig. 10 for the 2000 simulations of each scenario: (i) WSCC system (Fig. 10(a)); (ii) WSCC system and an oversized BES (Fig. 10(b)); (iii) WSCC system and an undersized BES without SIL (Fig. 10(c)); and (iv) WSCC system and an undersized BES with SIL (Fig. 10(d)). The maximum and minimum levels of the SOC of the battery in scenarios depicted in Figs. 10(c) and 10(d) have been set with the aim of obtaining a relatively high probability to reach energy saturation. As it can be observed from Figs. 10(a) and 10(b), using an oversized BES that never reaches energy saturations reduces the variations of $\omega_{\rm COI}$ by about 60% with respect to the system without storage. On the other hand, Fig. 10(c) shows that energy saturations of the BES causes oscillations that can even be larger than those in the system without battery, whereas Fig. 10(d) demonstrates that the inclusion of the SIL ($\mu = 0.2$) helps to reduce the amplitude of those oscillations, getting a similar performance than in the case with the oversized BES.

V. Conclusions

This paper proposes a simple and effective controller to smooth the transients that derive from energy saturations of ESSs. A novel control block for a BES is presented and tested through time domain analysis carried on a well-known benchmark system. Simulation results show that the proposed control is able to smooth abrupt oscillations caused by the energy saturation of the BES. The stochastic analysis shows that the proposed control allows reducing the size of the ESS while maintaining acceptable dynamic performance, thus leading to a reduction of the cost of the device. The simplicity of this control strategy, which only requires to set the maximum and minimum storable energy thresholds, allows to easily implement this control to all sorts of ESSs, such as Compressed Air Energy Storage (CAES) and Super Magnetic Energy Storage (SMES), among others.

Future work will focus on designing more advanced and robust control strategies able to improve the response of VSC-based ESSs and at the same time to reduce the size of the devices.

References

[1] H. Ibrahim, A. Ilinca, and J. Perron, "Energy Storage Systems - Characteristics and Comparisons," *Renewable and Sustainable Energy Reviews*, vol. 12, pp. 1221–1250, 2008.

[2] M. Beaudin, H. Zareipour, A. Schellenberglabe, and W. Rosehart, "Energy storage for mitigating the variability of renewable electricity sources: An updated review," *Energy for Sustainable Development*, vol. 14, pp. 302–313, 2010.

[3] "Electrical Energy Storage," white paper, IEC, Dec. 2011.

[4] A. Oudalov, R. Cherkaoui, and A. Beguin, "Sizing and Optimal Operation of Battery Energy Storage System for Peak Shaving Application," in *Power Tech, IEEE*, Lausanne, July 2007, pp. 621–625.

[5] P. Mercier, R. Cherkaoui, and A. Oudalov, "Optimizing a Battery Energy Storage System for Frequency Control Application in an Isolated Power System," *IEEE Transactions on Power Systems*, vol. 24, no. 3, pp. 1469–1477, Aug. 2009.

[6] X. Liu, A. Aichhorn, L. Liu, and H. Li, "Coordinated Control of Distributed Energy Storage System With Tap Changer Transformers for Voltage Rise Mitigation Under High Photovoltaic Penetration," *IEEE Transactions on Smart Grid*, vol. 3, no. 2, pp. 897 – 906, June 2012.

[7] K. Zhang, C. Mao, J. Lu, D. Wang, X. Chen, and J. Zhang, "Optimal control of state-of-charge of superconducting magnetic energy storage for wind power system," *IET Renewable Power Generation*, vol. 8, no. 1, pp. 58–66, Jan. 2014.

[8] M. G. Molina, P. E. Mercado, and E. H. Watanabe, "Improved Superconducting Magnetic Energy Storage (SMES) Controller for High-Power Utility Applications," *IEEE Transactions on Energy Conversion*, vol. 26, no. 2, pp. 444 – 456, June 2011.

[9] V. P. Singh, S. R. Mohanty, N. Kishor, and P. K. Ray, "Robust H-infinity load frequency control in hybrid distributed generation system," *Electrical Power & Energy Systems*, vol. 46, pp. 294–305, 2013.

[10] F. A. Inthamoussou, J. Pegueroles-Queralt, and F. D. Bianchi, "Control of a Supercapacitor Energy Storage System for Microgrid Applications," *IEEE Transactions on Energy Conversion*, vol. 28, no. 3, pp. 690–697, Sept. 2013.

[11] J. Fang, W. Yao, Z. Chen, J. Wen, and S. Cheng, "Design of Anti-Windup Compensator for Energy Storage-Based Damping Controller to Enhance Power System Stability," *IEEE Transactions on Power Systems*, vol. 29, no. 3, pp. 1175–1185, May 2014.

[12] E. Pérez, H. Beltran, N. Aparicio, and P. Rodríguez, "Predictive Power Control for PV Plants With Energy Storage," *IEEE Transactions on Sustainable Energy*, vol. 4, no. 2, pp. 482 – 490, Sept. 2012.

[13] S. Arabi and P. Kundur, "Stability Modelling of Storage Devices in FACTS Applications," in *Power Engineering Society Summer Meeting*, Vancouver, BC, July 2001, pp. 767–771 vol.2.

[14] D. N. Kosterev, "Modeling Synchronous Voltage Source Converters in Transmission System Planning Studies," *IEEE Transactions on Power Delivery*, vol. 12, no. 2, pp. 947–952, Apr. 1997.

[15] E. Uzunovic, C. A. Cañizares and J. Reeve, "Fundamental Frequency Model of Static Synchronous Compensator," in *29th North American Power Symposium (NAPS)*, Laramie, Wyoming, Oct. 1997, pp. 49–54.

[16] M. H. Ali, B. Wu, and R. A. Dougal, "An Overview of SMES Applications in Power and Energy Systems," *IEEE Transactions on Sustainable Energy*, vol. 1, no. 1, pp. 38–47, Apr. 2010.

[17] F. Milano, *Power System Modelling and Scripting*. London: Springer, 2010.

[18] F. Milano and R. Zárate Miñano, "Study of the Interaction between Wind Power Plants and SMES Systems," in *12th Wind Integration Workshop*, London, UK, Oct. 2013.

[19] C. M. Shepherd, "Design of Primary and Secondary Cells II. An Equation Describing Battery Discharge," *Journal of the Electrochemical Society*, vol. 112, no. 7, pp. 657–664, 1965.

[20] P. M. Anderson and A. A. Fouad, *Power System Control and Stability*, 2nd ed. Wiley-IEEE Press, 2003.

[21] F. Milano, "A Python-based Software Tool for Power System Analysis," in *Procs. of the IEEE PES General Meeting*, Vancouver, BC, July 2013.

[22] M. Perninge, V. Knazkins, M. Amelin, and L. Söder, "Risk Estimation of Critical Time to Voltage Instability Induced by Saddle-Node Bifurcation," *IEEE Transactions on Power Systems*, vol. 25, no. 3, pp. 1600–1610, Aug. 2010.

[23] F. Milano and R. Zárate Miñano, "A Systematic Method to Model Power Systems as Stochastic Differential Algebraic Equations," *IEEE Transactions on Power Systems*, vol. 28, no. 4, pp. 4537–4544, June 2013.

Álvaro Ortega (S'14) graduated from The Higher Technical School of Industrial Engineering, UCLM (Spain) - in 2013 with the Electrical and Electronic Itinerary and graduated with honors in his Final Project. His FP was about modeling and dynamic analysis of energy storage systems based on compressed air. He commenced his MSc in UCD in September 2013, within the Electricity Research Centre (ERC).

Federico Milano (SM'09) received from the University of Genoa, Italy, the Electrical Engineering degree and the Ph.D. degree in 1999 and 2003, respectively. From 2001 to 2002 he was with the University of Waterloo, Canada, as a Visiting Scholar. From 2003 to 2013, he was with the University of Castilla-La Mancha, Ciudad Real, Spain. In 2013, he joined the University College Dublin, Ireland, where he is currently an associate professor. His research interests include power system modeling,